POLITECNICO DI TORINO
Repository ISTITUZIONALE

Nonlinear elastic response of thermally damaged consolidated granular media

(Article begins on next page)

29 April 2024

Nonlinear elastic response of thermally damaged consolidated granular media

M. Scalerandi, M. Griffa, P. Antonaci, M. Wyrzykowski, and P. Lura

Additional information on J. Appl. Phys.

Nonlinear elastic response of thermally damaged consolidated granular media

M. Scalerandi,[1] M. Griffa,[2,a)] P. Antonaci,[3] M. Wyrzykowski,[2,4] and P. Lura[2,5]

[1]*Department of Applied Science and Technology, Institute of Condensed Matter and Complex Systems Physics, Politecnico di Torino, 10129 Torino, Italy*
[2]*Swiss Federal Laboratories for Materials Science and Technology (EMPA), Dübendorf 8600, Switzerland*
[3]*Department of Structural, Geotechnical and Building Engineering, Politecnico di Torino, 10129 Torino, Italy*
[4]*Department of Building Physics and Building Materials, Lodz University of Technology, 90-924 Lodz, Poland*
[5]*Institute for Building Materials, Swiss Federal Institute of Technology Zürich (ETHZ), 8093 Zürich, Switzerland*

The mechanical properties of consolidated granular media are strongly affected by large temperature changes which induce the development and localization of stresses, leading in turn to damage, e.g., cracking. In this work, we study the evolution of linear and nonlinear elasticity parameters when increasing the temperature of the thermal loading process. We prove the existence of a link between linear and nonlinear elasticity properties. We show that the change of the nonlinear elasticity parameters with the increase in the thermal loading is larger at the lower temperatures than the corresponding change for the linear parameters, suggesting that nonlinear elasticity can be exploited for early thermal damage detection and characterization in consolidated granular media. We finally show the influence of grain size upon the thermal damage evolution with the loading temperature and how this evolution is mirrored by the nonlinear elasticity parameters. © 2013 AIP Publishing LLC. [http://dx.doi.org/10.1063/1.4801801]

I. INTRODUCTION

Consolidated granular media, both natural (rocks) or man-made (building materials, e.g., concrete, and ceramics produced by sintering), exhibit a complicated, nonlinear elastic behavior. The observed phenomenology includes hysteresis in the stress-strain constitutive equation,[1–3] excitation amplitude-dependent resonance frequencies,[4–6] the generation of harmonics,[7] the loss of validity of the superposition[8,9] and reciprocity[10] principles, and conditioning/relaxation phenomena.[11–14]

Nonlinear elasticity parameters measured in various types of experiments are very sensitive to changes in the microstructure, including changes due to damage processes, e.g., cracking. Therefore, nonlinear elasticity measurements have been exploited for non-destructive detection and characterization of the microstructural evolution due to both intrinsic processes[15,16] and damage-related ones.[17,18] In the case of concrete, for instance, the evolution of nonlinear elastic properties has been exploited for studying mechanical,[19] corrosion-related,[20] and alkali silica reaction-related[6,21–24] cracking.

Thermal expansion-related cracking is a very common damage process in consolidated granular media such as concrete, where it is either due to the development of temperature gradients caused by the exothermal hydration reactions occurring during hardening and/or by "thermal loading" from the boundaries (gradients created from the outside), for example, in special infrastructures such as nuclear power plants or nuclear waste repositories.

The evolution of the microstructure in the presence of large spatial-temporal thermal gradients needs to be detected and characterized for improving models of the material's mechanical response and of its evolution in correspondence of different thermal loadings.[25–28] Together with the modeling improvement, the experimental detection of thermal damage in the early stages, when, e.g., cracks are not yet visible on the surface of the sample, is of paramount importance for preventive intervention.

Thermal expansion-related cracking usually occurs due to the development of highly heterogeneous stress fields in correspondence of temperature increases. Such cracking and the consequent changes in the macroscopic linear/nonlinear elastic behavior of a sample are functions of several physical parameters.

The first important parameters are the number of phases composing the material and the degree of heterogeneity in their thermo-mechanical properties. The spatial heterogeneity of the thermal expansion stresses is a direct consequence of the thermo-mechanical spatial heterogeneity.[29]

Other relevant parameters in thermal cracking are geometrical ones related with the microstructure. Computational modeling shows that thermal cracking is strongly dependent upon the spatial arrangement of the inclusions, their shape (all identical, e.g., spheres, or irregular, e.g., polygons), size and size distribution (monodisperse or polydisperse inclusions).[30] Thermal stresses tend to concentrate in regions of the matrix most closely surrounded by inclusions. In those regions, the stresses achieve larger values than in more "open" regions.[30] Given an identical inclusion spatial arrangement, identical inclusion shape and similar levels of heterogeneity, a larger inclusion size leads on average to

---

a)Author to whom correspondence should be addressed. Electronic mail: michele.griffa@empa.ch

smaller inter-inclusion distances, thus to larger thermal stresses when the temperature is increased.[30]

The size of the inclusions within the matrix of a composite medium may have an influence on the thermal cracking process not only because of its effects on the average inter-inclusion distance. Experiments about drying shrinkage, a process similar to thermal cracking due to the inclusion-related restraining mechanisms at play, performed by Bisschop and Van Mier with model cement-based composites, showed that the total cumulative length and depth of the cracking network increased with the aggregate size.[31]

The environmental conditions during the sample preparation and development (consolidation for rocks, setting and hardening for concrete) strongly affect the microstructure geometry as well, for example, by influencing the degree of generation of air voids, cracks, and interfaces.

In this work, we investigate the evolution of the linear and nonlinear elastic behaviors with the magnitude of the thermal load (temperature achieved), adopting cementitious materials as models of consolidated granular media.

A cement-based material can be thought of as a complicated multi-phase composite. Cement-based materials are made of grains (inclusions), called aggregates, embedded in a matrix (cement as a binder). The mechanical and thermal properties of both components (aggregates and hydrated cement) are highly spatially heterogeneous. This is due to the heterogeneity of the matrix, composed of different hydration phases, porosity and air inclusions, and heterogeneity of the aggregates. The advantage in using cement-based materials as model systems is the possibility of producing them in the laboratory with a large degree of design and control of physical and geometrical properties.

The two main parameters we investigated in this study are the aggregate size and method of mixing, the latter leading to different amounts of air inclusions within the matrix.

The development of large and localized stresses in cement-based materials during thermal loading is not only related to thermal expansion but also to shrinkage induced by chemical processes occurring at high temperatures, mainly dehydration. Dehydration comes with radical microstructural changes which, on one side, contribute even more to create spatial and material heterogeneity, on the other side lead to shrinkage processes that contribute to the cracking as well.

The sample preparation and the thermal loading protocols are described in Sec. II. The results of the linear/nonlinear elasticity measurements, at different stages of the thermal loading protocols, are presented in Sec. III. The relevance of the results for the characterization of thermal cracking in a non-destructive fashion is discussed in Sec. IV.

II. EXPERIMENTAL CAMPAIGN

A. Sample preparation

We used mortar samples of size $25 \times 25 \times 100 \, \text{mm}^3$ (height, width, and length, respectively) as model systems of consolidated granular materials. Mortar is analogous to concrete except for the use of small size (below $4 \, \text{mm}$) rock aggregates, mixed together with water and cement. The samples were all cast at the same time. They were all prepared with the same mixture design except for the aggregate size range and the type of mixing.

The used cement was ordinary Portland cement (CEM I 42.5N). The aggregate used was alluvial sand from Switzerland, with well-rounded particles and dry density of $2659 \, \text{kg} \, \text{m}^{-3}$. The amount of aggregates in the mortar was about 40% by volume, corresponding to a cement-to-aggregate ratio (c/a) by mass fraction of 0.917. Deionized water was used as mixing water in an amount corresponding to a water-to-cement ratio (w/c) of 0.3 by mass (including the superplasticizer, see below).

Relatively low w/c allows obtaining mortar with high mechanical strength and low fluid permeability. A similar mortar produced with the same w/c and with the same amount and type of aggregates achieved a compressive strength of 88 MPa and a Young modulus in compression of 34 GPa after 28 days of maturing in sealed conditions.[32]

Due to a low w/c and a high amount of solids (cement and aggregates), a liquid polycarboxylate-based superplasticizer (SIKA VC 3082) was added to mixing water in an amount of 0.5% by cement weight. This allowed obtaining better workability of the mixture.

We prepared a total of eight specimens of equal size and equal *c/a*. Four of them had aggregates with size in the range $0.25 - 1 \, \text{mm}$. The remaining four specimens were prepared with aggregates in the range $1 - 4 \, \text{mm}$. For each aggregate size range, we realized two samples with a standard open-air mixer (planetary mixer of $5 \, l$ volume by Hobart), while the remaining two were made with a vacuum mixer (Twister Evolution of $0.5 \, l$ volume by Renfert).

When mixing is performed in contact with the normal room environment, air bubbles are naturally entrapped in the mixture, resulting in large (from a few 10 to 100 μm) spherical air voids in an average amount of about 1%–3% of hardened mortar volume. We observed large spherical air voids with diameter up to about 1 mm by optical microscopy of polished cross-sections from samples of the same size and prepared with open-air mixing.

Vacuum mixing, performed in our case at nominal pressures of 870 mbar, allows for decreasing the number of such large air voids. For each sample type, we estimated the air void volume fraction by the method described in Appendix A. Samples prepared with open-air mixing had an air void average volume fraction of 1.38% and 1.57%, respectively, in correspondence of the smaller and larger aggregates. Samples prepared with the vacuum mixing had air void average volume fraction of 0.43% and 0.34%, again for smaller and larger aggregates, respectively. Air voids may be either beneficial or not depending upon the aimed material properties. For instance, they reduce the compressive strength and the Young modulus.

After mixing and casting, the samples were left initially for 1 day in a climatic chamber at relative humidity (RH) $\geq 95\%$ and temperature of $20 \pm 0.5 \, ^\circ\text{C}$, then they were unmolded, sealed with plastic envelopes, and moved into another climatic chamber at $20 \pm 0.5 \, ^\circ\text{C}$ and $90\% \pm 5\%$ RH for further curing. The total curing time was 1 month, before

the start of the thermal loading protocol and the respective measurements described in Sec. II B.

After the 1 month-long curing, the eight samples were finally sorted out and labelled according to a three-field code, where the first field indicates the mixing technique (A = open-air, V = Vacuum), the second field denotes the higher limit of the aggregate size range (1 or 4 mm), and finally, the third field identifies the specimen (a or b).

B. Experimental procedure

We performed measurements on the samples described in Sec. II A in their initial ("intact") state, at room temperature, and after each thermal loading step. Each thermal loading step lasted 3 h. The oven was pre-heated before starting the loading step. After heating, the samples were let cool down for 24 h in indoor environment, at ambient temperature ranging from 15 °C to 26 °C and at room RH (not monitored). The measurements were then performed within 1 h. After measuring, we moved back the samples to the oven for the next step. The piezoelectric transducers for the measurements were removed from the specimens after each measurement and before each next thermal loading step, so as not to damage them. Then they were attached again, after the sample cooling, for the subsequent ultrasonic measurement session.

Temperatures of 120 °C, 180 °C, and 350 °C were chosen for the successive thermal loading steps. At such temperatures, the mortar undergoes different microstructural changes. At the lower temperatures (around 100 °C), the free water is lost from the pores and dehydration of some of the hydration products, e.g., ettringite, takes place. At temperatures around 350 °C, the majority of the principal hydration product, calcium-silicate-hydrates (C-S-H), is fully dehydrated.[33,34]

Dehydration leads to shrinkage. Together with the increase and localization of internal stresses due to thermal expansion, shrinkage is a source of cracking. In addition, we expect that cracking occurred as well after each thermal loading step, before performing the measurements on the samples, as a consequence of the cooling down to room temperature and the associated thermal contraction.

During each thermal loading step, the temperature was kept approximately constant, with fluctuations of the order of ±5 °C during the whole duration of the step. Thermal loading was always repeated twice, successively, at the same temperature (except at 350 °C) before moving to the next step.

At the end of each step, after the cooling, we performed linear and nonlinear elasticity measurements based upon ultrasonic pulse transmission.

Two piezoceramic, longitudinal ultrasonic transducers of the same type (Dakel MTR 15), one acting as emitter and the other as receiver, were attached to the opposite ends, along the longitudinal dimension, using phenyl-salycilate as a coupling agent. The transducers have a diameter of 25 mm and a flat frequency response in the range 50–550 kHz. The emitter, connected to a waveform generator via a 20×, fixed

gain, broadband (DC up to about 1 MHz) linear amplifier, was used to inject pulses into the samples.

We used two types of input waveforms: bursts (Fig. 1(a)), i.e., sinusoidal pulses composed of 10 cycles at central frequency $\nu = 200$ kHz and repetition frequency of 1 Hz, for the nonlinear elasticity measurements, and short (1 μs-long) pulses at a repetition rate of 50 Hz for the linear measurements.

The pulses were transmitted through the samples along the longitudinal dimension (approx. 100 mm travel path). After each thermal loading step and the following cooling down to room temperature, the pulse transmission measurements were repeated. The linearity of the whole measurement system was carefully tested before performing the ultrasonic experiments. The nonlinear elasticity measurements consisted in injecting the sinusoidal bursts in correspondence of 15 increasing amplitudes of excitation (ranging between 2 V and 200 V, after the fixed-gain amplification), while the linear measurements were performed at a single excitation amplitude (1 V).

The excitation, propagating through the sample, was recorded by the receiver and transferred to a digitizing oscilloscope (Agilent Infiniium DSO8064A) used for data acquisition. The sampling rate was set to 10 MS/s, thus providing sufficient data points in one period for the data analysis. The recorded signals were 0.5 ms long. Only a small (initial) part of the recorded signals was used for the data analysis. Data acquisition was repeated 10 times for each pulse injection, at each excitation amplitude. The recorded signals were averaged to reduce noise effects. In principle, such averaging could be negatively affected by conditioning effects taking place between the last and the first measurements. However, as shown by Gliozzi *et al.*,[13] conditioning in concrete is not instantaneous. Several pulses of the form used here are needed to provide appreciable effects on the measurements of the scaling subtraction method (SSM) indicator. We have calculated the SSM indicator as well for each of the 10 signals corresponding to each excitation amplitude. We have observed only slightly differences and absolutely no trend in the overall behavior, thus confirming that eventual conditioning effects fall below the noise level.
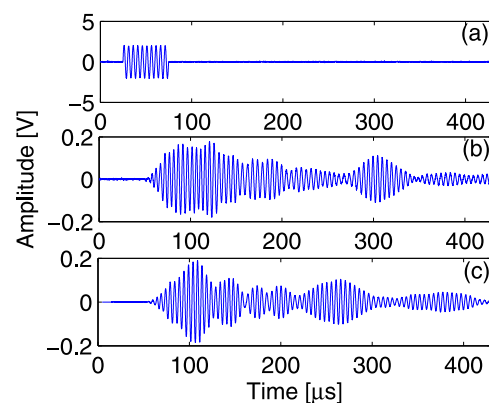

FIG. 1. Source (a) and output signals (b) and (c) in correspondence of the lowest excitation amplitude during the nonlinear elasticity measurements on sample A1a. The signal in (b) is before the first thermal loading step at 120 °C, while the one in (c) after.

Examples of averaged recorded signals during the non-linear measurements are shown in Figs. 1(b) and 1(c), for the sample A1a, respectively, before and after the first thermal loading step at 120 °C. The remarkable change in the waveform from the intact state to the one after the first thermal loading step is mostly due to cracking and other microstructural changes related with a combination of thermal deformations, dehydration, and drying shrinkage.

1. Linear elasticity measurements: Time-Of-Flight

The linear elasticity measurements on each sample, after each thermal loading step, were performed at low excitation amplitude in order to induce as less as possible nonlinear elastic effects. These measurements were indirect and consisted in estimating the travel time (Time-Of-Flight, TOF) of the first arrival of the short pulse transmitted from one side to the other of the sample. Such TOF, Δt, is

$$\Delta t = L \cdot \sqrt{\frac{\rho}{K + \frac{2}{3} \cdot G}}, \qquad (1)$$

where L is the sample length, ρ its mass density, and K and G the linear bulk and shear elastic moduli, respectively. For each pulse transmission, the TOF was measured directly on the recorded signal as the first time instant when the signal increases above the noise level.

2. Nonlinear elasticity measurements: The scaling subtraction method

We used the ultrasound pulse transmission measurements at multiple, increasing excitation amplitudes for the determination and characterization of the nonlinear elastic response of the samples after each thermal loading step. The nonlinear elastic response relates with the damage level. The data analysis was performed entirely in the time domain, using the SSM,[8,9] in order to take full advantage of an optimal nonlinear-to-linear signal ratio.[35] This method is based on the loss of amplitude proportionality between the input and output signals. It differs from other nonlinear elasticity techniques belonging to the class of nonlinear elastic wave spectroscopy (NEWS) for exploiting the full nonlinear elastic frequency response of a damaged sample.[8,9]

Many NEWS techniques consist in exciting a sample with one or more high amplitude harmonic waves and in analysing the frequency spectrum of the signal due to the wave propagation. As a consequence of the nonlinear elastic behavior, the output signal's spectrum contains more frequencies than those of the excitation signals.[17] In such NEWS techniques, the nonlinear elastic effects on the propagated wave component at the same central frequency(ies) as the excitation(s) are not taken into consideration. These effects, in the form of amplitude dependence of the wave phase velocity and wave attenuation, are taken into account by the SSM method. They provide the SSM method with higher sensitivity to changes in the nonlinear elastic response than what achieved with other NEWS methods, where higher order harmonics or nonlinear wave mixing components have

usually low amplitudes and their changes with the nonlinear elastic response may be difficult to detect.

We indicate with $v_i(t)$, $\forall i = 1, ..., 15$, the signal recorded by the receiver in correspondence of the increasing excitation amplitude A_i, after a certain thermal loading step. The data analysis with these signals proceeds as follows:

1. For each excitation amplitude of the source signal, a reference, linear signal is defined as $v_i^{ref}(t) = \frac{A_i}{A_1} \cdot v_1(t)$; the working hypothesis here is that the lowest excitation amplitude is small enough not to excite the nonlinearity of the sample; thus, the reference signal would correspond to the response of the sample excited at amplitude A_i if it was perfectly linear elastic.
2. For each excitation amplitude of the source signal, a "nonlinear response signal" is calculated as $w_i(t) = v_i(t) - v_i^{ref}(t)$.
3. For each excitation amplitude A_i, $\forall i = 1, ..., 15$, the maxima x_i and θ_i of the absolute value of the output and nonlinear signals ($v_i(t)$ and $w_i(t)$), respectively, are calculated within a short time window after the first pulse arrival; θ_i is then plotted vs x_i and the curve is best fitted with a power law function of the type $\theta_i = a \cdot (x_i)^b$. The best fit parameter a essentially estimates the "strength" or "magnitude" of the nonlinear elastic response, while the parameter b is more related with the type.[8,9] The choice of a power law function is suggested by experimental observations and analytical models showing different scaling relationships existing between variables estimating the nonlinear elastic response ("nonlinear elastic indicators") and variables estimating the linear elastic one, at increasing excitation amplitudes. For example, the amplitude of the nonlinearly generated higher order harmonics (nonlinear indicator) usually scales with the amplitude of the strain wave (linear indicator), being the power law exponent dependent upon the harmonic order and the type of nonlinear elastic behavior.[17] The variable θ is used in this work as the nonlinear elastic indicator.

In Fig. 2, the procedure is illustrated for sample V4b after thermal loading at 120 °C. Figure 2(a) shows the output signal $v_i(t)$ (solid red line) and the corresponding reference signal, $v_i^{ref}(t)$ (dashed blue), in correspondence of the *ith* excitation amplitude, A_i, with $i = 8$ and $A_i = 120$ V. The differences between the two output signals can be hardly appreciated. However, when considering the nonlinear signal w_i (Fig. 2(b)), its well defined waveform clearly emerges from the noise level. Note that the nonlinear signal manifests itself only for high excitation amplitudes, as it should be expected. Finally, as shown in Fig. 2(c), the nonlinear indicator θ increases nonlinearly as a function of the maximum of the output signal x. In the adopted dB ($20 \cdot \text{Log}$) scales, a straight line can be observed, indication of a power law behavior (here the exponent is $b = 2.02$). We remark that a shift of such a power law curve towards the left corresponds to an increase in the value of the power law best fit parameter a, i.e., an increase in the "magnitude" of the nonlinear elastic response. Points corresponding to the lowest excitation amplitudes are not fitted well since they are known to be
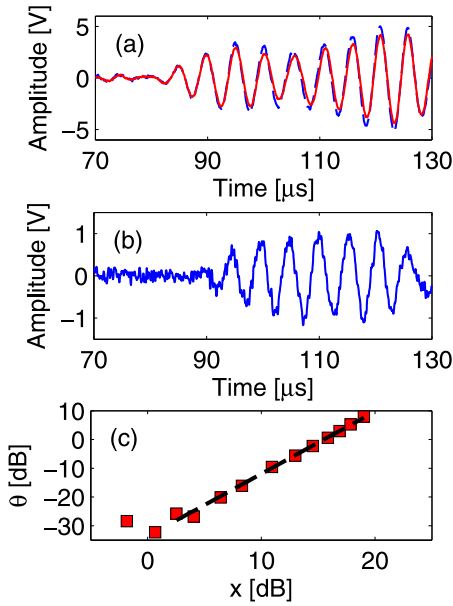
FIG. 2. Example of SSM signals and respective analysis, with the data recorded for sample V4b after the first thermal load at 120 °C. (a) Recorded output signal ($v_i(t)$, solid red line) and corresponding reference, "linear" signal ($v_i^{ref}(t)$, dashed blue line) at the *ith* excitation amplitude ($i = 8$), in this case equal to 120 V. (b) Nonlinear signal $w_i(t)$ built from the difference between the signals of subplot (a). (c) Curve of the nonlinear indicator $\theta = \max(|w|)$ vs the linear indicator $x = \max(|v|)$. On each axis, the base-10 logarithm of the respective variable, multiplied by 20, is plotted. Each point in the plot corresponds to a given excitation amplitude. The dashed line is the power law best fit line of the data.

FIG. 3. Nonlinear indicator θ vs the output amplitude x, at increasing thermal loads. The two variables are expressed in dB ($20 \cdot \mathrm{Log}$ of the value). (a) Results for one sample with large aggregates (A4a). (b) Results for one sample with small aggregates (A1a). Both the considered samples were produced with open-air mixing. In both plots (a) and (b), the dashed line represents power law best fits of the curves.

influenced by noise effects and therefore cannot be related to the sample nonlinearity.[35]

III. RESULTS

A. Aggregate size

In Fig. 3, we show the effects of the aggregate size on the thermal damage as mirrored by the nonlinear elastic behavior of the samples. We consider there two samples produced by open-air mixing and thermally loaded with the prescribed protocol: one with large aggregates (Fig. 3(a)); the other with small ones (Fig. 3(b)).

First of all, it is important to notice the significant nonlinearity manifested by the intact samples themselves, in both cases (circles). As mentioned in Sec. II B 2, a power law-like relationship between θ and x, with a power law exponent greater than 1, as in Fig. 3, indicates a nonlinear elastic behavior.

In both plots, we observe that for the largest excitation amplitude the nonlinear signal amplitude is only about 12 dB lower than the recorded output signal. Thus, the SSM method, as expected, allows to achieve a significant nonlinear-to-linear signal ratio. Such ratio can be simply calculated in correspondence of each excitation amplitude $A_i, \forall i = 1, ..., 15$, as the difference between the θ value and the x value in the dB scales used for the plots in Fig. 3.

The two samples exhibit a very similar scaling between θ and x, with a slightly larger attenuation for the large aggregate sample. Indeed, the received signals for the larger aggregate samples have amplitude in general smaller than
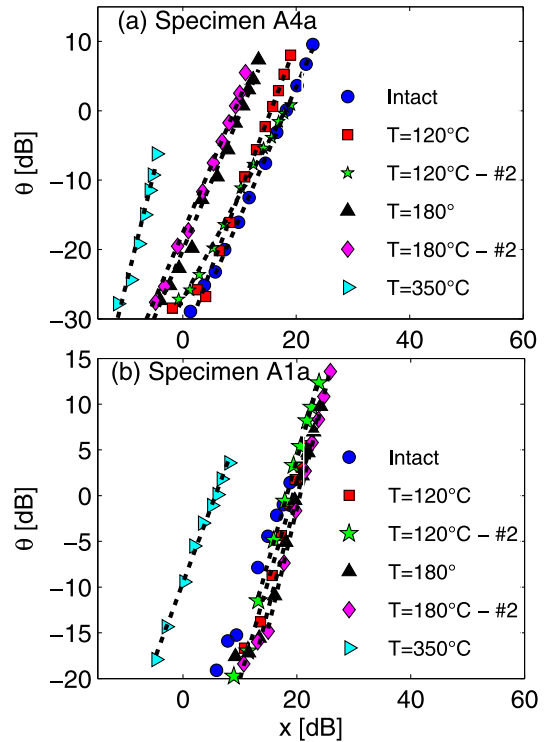
the amplitude of the corresponding signals for the smaller aggregate samples. We remark that this effect is independent of the excitation amplitudes, which were the same for all the samples. This effect is also manifested for all the loading steps, therefore cannot be ascribed to accidental variations in the pulse injection/recovery by the transducers, due to the possible difference in the transducer coupling. In this regard, we recall here that the transducers had to be removed and then reattached at each loading step.

If we consider the evolution of the nonlinear elastic response with the thermal loading temperature, the two samples behave differently. In both cases, a thermal load at 120 °C does not cause significant changes in the nonlinear parameters. Likewise, for both samples and for each value of loading temperature, repeating the thermal load does not induce significant variations either, thus indicating that cracks already present after the previous thermal load, at the same temperature, allow for thermal expansion without the generation of further large and localized stresses in the samples. On the contrary, while in the case of samples with large aggregates, the nonlinear response increases significantly in magnitude already after heating at 180 °C, the first significant variation in the nonlinear elastic response magnitude is observed for the samples with small aggregates only when a temperature of 350 °C is achieved.

It is important to note also that the nonlinear-to-linear signal ratio is much larger in Fig. 3(a) than in Fig. 3(b). For example, at 350 °C and for the largest excitation amplitude, the ratio θ/x is about -1.6 dB for the large aggregate sample

while it is -4 dB for the small aggregate one. In addition, as better discussed in Sec. III B, the θ vs x curves for all the samples are roughly parallel in the dB-dB plot, with a slope close to 2, which means a power law with exponent $b = 2$. It is worth recalling here that such a value for the power law exponent provides an indication of hysteretic elasticity, a specific type of nonlinear elasticity.[1] However, at least for the case of the largest thermal load and for the large aggregate size (right triangles in Fig. 3(a)), the exponent is clearly higher than 2.

Figure 4 shows the results for all four samples of each aggregate size. For the sake of clearness of the plots, results after repetition of the thermal load at the same temperature are not shown, but, as remarked before, in all cases no significant variation due to the repetition was observed. In Fig. 4, a single color is associated to a given sample, while different symbols are assigned to different thermal loads, as shown in the legend. In Fig. 4(a), red and magenta symbols refer to samples prepared with open-air mixing, while blue and green to samples prepared with vacuum mixing. In Fig. 4(b), red and green symbols refer to samples prepared with open-air mixing, while blue and magenta to samples prepared with vacuum mixing. The high reproducibility of the nonlinear elastic response evolution for each sample of the same type is remarkable, thus proving furthermore the absence of any
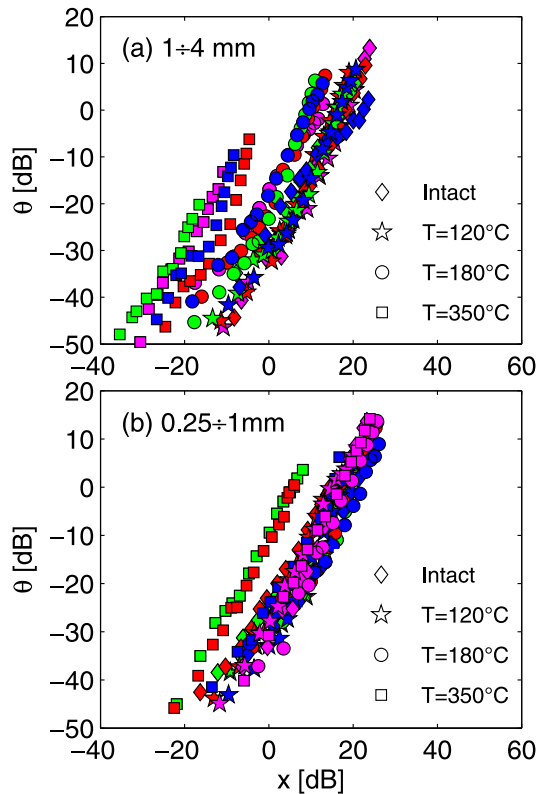
bias effects associated with the experimental setup and corroborating the significance of the measurements in absolute terms. As better discussed in Sec. III B, we observe almost no difference in the nonlinear elastic behavior of samples with large aggregate size produced with different mixing, while the samples with small aggregate size and prepared with open-air mixing exhibit a large increase in the nonlinear behavior, in correspondence of the increase from 180 °C to 350 °C.

B. Mixing technique

We consider here the influence of a smaller/larger volume fraction of air voids on the response to thermal loading. In Fig. 5, we compare the results for all the samples, again omitting results referring to repeated measurements at the same temperature. Data for the open-air mixing and for the vacuum mixing are reported in Figs. 5(a) and 5(b), respectively. In Fig. 5, curves with the same symbols correspond to the same thermal load temperature, as reported in the legend. Results for the two large aggregate samples are in magenta and red, while blue and cyan symbols refer to small aggregate size. From Fig. 5, we can infer that the mixing production technique has no substantial influence on the nonlinear elastic response of both small and large aggregate size
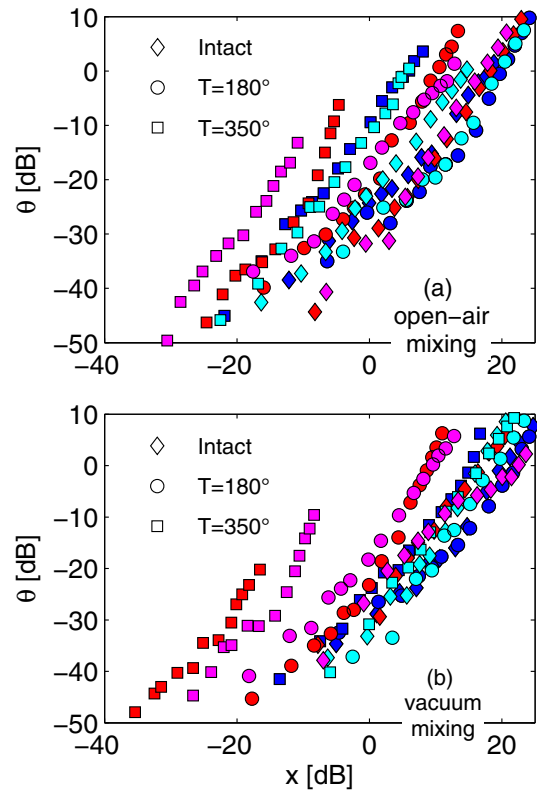

FIG. 4. Nonlinear indicator θ vs the output amplitude x at increasing thermal loads. (a) Results for all samples with large aggregate size. Magenta and red symbols refer to samples produced with open-air mixing; blue and green symbols refer to samples produced with vacuum mixing. (b) Results for all samples with small aggregate size. Green and red symbols refer to samples produced with open-air mixing; blue and magenta symbols refer to samples produced with vacuum mixing. Different symbols represent different thermal loading levels. Curves after the repetition of a thermal loading at the same temperature are not shown.

FIG. 5. Nonlinear indicator θ vs the output amplitude x at increasing thermal loads. (a) Results for samples produced with open-air mixing (magenta and red symbols refer to samples with large aggregate size; blue and cyan symbols refer to samples with small aggregate size). (b) Results for samples produced with vacuum mixing (magenta and red symbols refer to samples with large aggregate size; blue and cyan symbols refer to samples with small aggregate size). Different symbols represent different thermal loading levels. Curves after the repetition of a thermal loading at the same temperature are not shown.

samples. The only difference between the two datasets consists in the nonlinear elastic response change of the small aggregate samples when moving from the damage state at 180 °C to the one at 350 °C: the samples produced with vacuum mixing exhibit no significant change while those produced with open-air a more significant one.

C. Linear elastic measurements

Regarding the linear elastic measurements, we focus only on the samples with large aggregate size since the nonlinear elastic measurements show that appreciable changes occur while increasing the loading temperature predominantly for such samples. In Fig. 6(a), the TOFs are reported as a function of the thermal loading step temperature. As mentioned in Sec. II B 1, a TOF increase corresponds to a decrease in the linear elastic moduli. Figure 6(a) shows that the linear elastic moduli decrease with the successive thermal loading at increasing temperatures.

IV. DISCUSSION

The results presented in Sec. III allow to conclude that the aggregate size is a key parameter in controlling the thermal damage evolution, as evinced by the nonlinear elastic behavior changes with the thermal loading. In particular, samples with large aggregates tend to manifest a noticeable increase in the nonlinearity since the very beginning of the thermal loading process and their nonlinearity evolution with thermal loading is characterized by gradual, smooth transitions. Conversely, samples with small aggregates display a more "brittle" behavior in terms of nonlinearity, in the sense that the nonlinearity due to thermal damage appears only at larger temperatures, with a sudden transition. Unlike the aggregate size, the volume fraction of air voids, within the
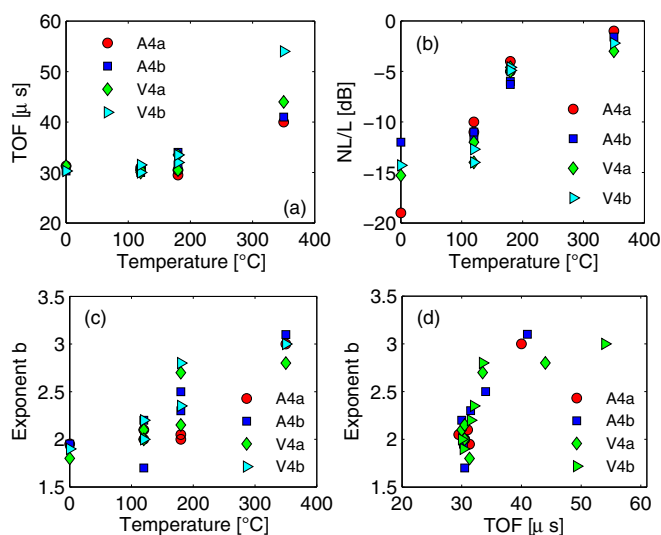

FIG. 6. Samples with large aggregate size. (a) TOF vs temperature of the thermal loading (duplicated symbols correspond to the repetition of the loading steps at the same temperature). (b) Nonlinear-to-linear signals ratio (in *dB*) vs the temperature of the thermal loading. (c) Exponent of the power law best fit for the θ vs x curves, plotted against the thermal loading temperature. (d) Power law exponent vs TOF. Different symbols refer to different samples.

ranges achieved in this work, does not seem to affect the nonlinearity evolution as much as the aggregate size does. The reason for this may consist in the small difference in air void volume fraction between the two categories of samples, those produced with the open-air mixing and those with vacuum mixing. Air entraining additives should be used to achieve larger volume fraction values (order of 8%−10%).

The decrease in the linear elastic moduli with the loading temperature (Fig. 6(a)) appears to be significant only for the transition to the highest thermal load. This result indicates that linear elastic moduli have low sensitivity to progressive damage at the lower temperatures (between 100 °C and 200 °C). All of these results are in agreement with others reported in the literature for granular media.[36,37] We notice that the repeatability of the TOF measurements after the first and second thermal loads at the same temperature is very remarkable. The change in TOF is more evident for samples produced with vacuum mixing (diamond and triangle symbols).

For the same set of samples, we also calculated the non-linear-to-linear (NL/L) signal ratio at the largest excitation amplitude, defined as the maximum of the absolute value of the nonlinear signal w divided by the maximum of the absolute value of the recorded signal v, reported in Fig. 6(b) in the same *dB* scales as used in Figs. 3–5. Finally, we also calculated the exponent of the θ vs x power law best fit, reported in Fig. 6(c). The NL/L ratio increases at successive thermal loads, with larger increase rate in correspondence of the initial loads. The increase rate is larger than the TOF one, in agreement with results reported in the literature.[27] This result indicates that the nonlinear-to-linear signal ratio is another parameter very sensitive to the initial development of thermal damage, at temperatures just above 100 °C.

Even more interesting is the dependence of the power law exponent on the thermal load. We recall here that the power law best fit has been performed neglecting in all cases points corresponding to measurements at low excitation amplitudes. At low excitation amplitudes, the slope of the curve is close to 1, thus indicating that noise effects might be dominant.[35] For large and increasing thermal load temperatures, we generally observe an increase of the exponent from 2 to 3. The increase in the exponent value is quite regular, and it is known to be an indication of microstructural changes due to the appearance of different nonlinear features, such as cracks/joints behaving as clapping interfaces during the passage of large strain elastic waves.[38,39]

Figures 6(a) and 6(c) show that both the TOF and the power law exponent are positively correlated with the loading temperature. Figure 6(d) shows that the two variables are also well correlated with each other. However, the rate of increase with the loading temperature is negatively correlated. With increasing loading temperature, the TOF undergoes the most significant changes only at large temperatures, while the power law exponent exhibits the opposite trend (the largest increases are achieved for steps already at the lower temperatures). Figure 6(d) thus indicates that linear elasticity measurements start to exhibit sensitivity to the increase in the thermal damage only when high temperatures are achieved. On the contrary, nonlinear elasticity measurements show to

be most sensitive at low temperatures, already below 200 °C, thus at low damage levels.

We remark that we also performed an additional thermal loading at a higher temperature (650 °C). In this case, all the samples exhibited very large damage expressed on the surface in the form of visible cracks. Such large damage levels prevented obtaining a reliable coupling between the samples and the transducers. Thus, although we could not perform any ultrasonic test, we expect large nonlinearity to be present and damage to be independent from both aggregate size and specimen preparation.

Attenuation also deserves attention in the context of thermal damage. Since the excitation amplitudes were always the same, the amplitude of the output signal expressed in decibels, dB, (the x variable) in Figs. 3–5, conveys information about attenuation. We note that a decrease of the Q-factor is evident for the damaged samples and it is quantified as up to 30 dB down in the amplitude of the received signal. We also expect a significant dependence of the Q-factor from the amplitude of excitation, but this analysis is out of the scope of the work reported here. From the linear elasticity point of view, we observe that attenuation is almost independent from the grain size in the intact state but, being linked to damage, is much different for large and small grain sizes after the successive thermal loadings (see Fig. 4). The mixing technique seems not to have a significant influence on the Q-factor (see Fig. 5).

V. CONCLUSIONS

The effect of successive, thermal loading steps, at different temperatures, on the elastic response of consolidated granular materials to ultrasound excitation has been analyzed as a function of grain size and sample preparation; different sample preparation methods leading to different amounts of spherical air voids. We chose mortar, a cementitious building material, as a model system of a consolidated granular material.

The preparation technique (open-air or vacuum mixing) seems not to have any significant influence on the material behavior, since the air void content did not vary significantly. On the contrary, our results show that the aggregate size is a very relevant parameter. Samples with large (1–4 mm) aggregates display a large increase in the nonlinear elastic response during the early stages of the thermal loading, at the lower temperatures. The nonlinearity evolution with thermal loads is characterized by gradual transitions for samples with large aggregates. On the contrary, samples with smaller (0.25–1 mm) aggregates show significant changes in the nonlinear elastic response only at larger temperatures, with a sudden transition when going from 180 °C to 350 °C.

For the samples with large aggregates, we found a clear correlation between the exponent of the power law fitting functions and the measured Time-of-Flight, which we adopted as a parameter representing linear elastic properties. Both parameters increase with the successive thermal damage steps, at increasing temperatures. However, while the Time-of-Flight appreciably increases only in correspondence at the higher temperatures, the power law exponent exhibits

the larger increase at the lower temperatures. This indicates that such a nonlinear elastic parameter is very sensitive to thermal damage occurring already in correspondence of thermal loading at temperatures just above 100 °C, while linear elastic parameters, like linear elastic moduli, seem to be sensitive only to damage evolution after a certain degree of damage has already been accumulated.

Our results, obtained by tracking the nonlinear elastic response evolution with the thermal damage of the same samples at the different temperatures, confirm those of Payan *et al.* obtained on distinct samples damaged at different temperatures[27] and they suggest the possibility of higher sensitivity of nonlinear elasticity based-methods in the detection and characterization of thermal damage already obtained at low temperatures, just above 100 °C.

ACKNOWLEDGMENTS

APPENDIX A: AIR VOID VOLUME FRACTION MEASUREMENT

The air void volume fraction was estimated by adapting the procedure indicated in the German European Standard protocol nr. DIN EN 480-11. Additional samples of the same type as used for the thermal damage measurements were produced following the same procedures described in Sec. II A, for each aggregate size and with each mixing method. One sample of each type was chosen from such spare samples. The sample was halved along its longitudinal direction, and the internal cross-section, 100 mm long, of one half was polished with sand paper of decreasing roughness. After polishing, the same half sample was dried in an oven at 50 °C for 30 min. Then, the internal cross-section surface was colored with black ink and dried in the same oven for additional 30 min. After drying, the polished and black-colored surface was covered with talc powder. Talc powder grains fill in the air voids. The surface was then put in a flat bed optical scanner to acquire an image of the polished cross-section with pixel size equal to 10 μm. The recorded red-green-blue (RGB) image was then binarized via the manual choice of a threshold: pixel values above the threshold were re-defined as white (talc), and pixel values below the threshold were re-defined as black. The ratio between the number of white pixels and the total number of pixels in the binary image was taken as an estimate of the air void volume fraction.

[1] R. A. Guyer, J. TenCate, and P. A. Johnson, Phys. Rev. Lett. **82**, 3280 (1999).
[2] K. E. Claytor, J. R. Koby, and J. TenCate, Geophys. Res. Lett. **36**, L06304, doi: 10.1029/2008GL036978 (2009).
[3] G. Renaud *et al.*, J. Acoust. Soc. Am. **130**, 3583 (2011).
[4] A. Kadish, P. A. Johnson, and B. Zinszner, J. Geophys. Res. **101**, 25139, doi: 10.1029/96JB02480 (1996).
[5] M. Bentahar, H. El Aqra, R. El Guerjouma, M. Griffa, and M. Scalerandi, Phys. Rev. B **73**, 014116 (2006).
[6] J. Chen *et al.*, J. Acoust. Soc. Am. **130**, 2728 (2011).

[7]K. Van den Abeele and J. De Visscher, Cem. Concr. Res. **30**, 1453 (2000).

[8]M. Scalerandi, A. S. Gliozzi, C. L. E. Bruno, D. Masera, and P. Bocca, Appl. Phys. Lett. **92**, 101912 (2008).

[9]C. L. E. Bruno, A. S. Gliozzi, M. Scalerandi, and P. Antonaci, Phys. Rev. B **79**, 064108 (2009).

[10]M. Scalerandi, A. S. Gliozzi, and C. L. E. Bruno, J. Acoust. Soc. Am. **131**, EL81 (2012).

[11]J. A. TenCate *et al.*, Phys. Rev. Lett. **93**, 065501 (2004).

[12]M. Scalerandi, A. S. Gliozzi, C. L. E. Bruno, and P. Antonaci, Phys. Rev. B **81**, 104114 (2010).

[13]A. S. Gliozzi, M. Scalerandi, P. Antonaci, and C. L. E. Bruno, Appl. Phys. A **100**, 421 (2010).

[14]M. Scalerandi, A. S. Gliozzi, C. L. E. Bruno, and P. Antonaci, J. Acoust. Soc. Am. **131**, 4304 (2012).

[15]J.-C. Lacouture, P. A. Johnson, and F. Cohen-Tenoudji, J. Acoust. Soc. Am. **113**, 1325 (2003).

[16]K. Van Den Abeele, W. Desadeleer, G. De Schutter, and M. Wevers, Cem. Concr. Res. **39**, 426 (2009).

[17]K. Van den Abeele *et al.*, Res. Nondestruct. Eval. **12**, 17 (2000).

[18]I. Solodov and G. Busse, Appl. Phys. Lett. **91**, 251910 (2007).

[19]P. Antonaci, C. L. E. Bruno, P. G. Bocca, M. Scalerandi, and A. S. Gliozzi, Cem. Concr. Res. **40**, 340 (2010).

[20]P. Antonaci, C. L. E. Bruno, M. Scalerandi, and F. Tondolo, "Effects of corrosion on linear and nonlinear elastic properties of reinforced concrete bars," Cem. Concr. Res. (submitted).

[21]M. Sargolzahi, S. A. Kodjo, P. Rivard, and J. Rhazi, Constr. Build. Mater. **24**, 1398 (2010).

[22]J. Chen, A. R. Jayapalan, J.-Y. Kim, K. E. Kurtis, and L. J. Jacobs, Cem. Concr. Res. **40**, 914 (2010).

[23]A. S. Kodjo *et al.*, Cem. Concr. Res. **41**, 422 (2011).

[24]K. Lesnicki *et al.*, NDT & E Int. **44**, 721 (2011).

[25]W. Li, W. Sun, and J. Jiang, Mag. Concrete Res. **64**, 35 (2012).

[26]M. Petkowski, Cem. Concr. Res. **40**, 1744 (2010).

[27]C. Payan, V. Garnier, J. Moysan, and P. A. Johnson, J. Acoust. Soc. Am. **121**, EL125 (2007).

[28]C. de Sa and F. Benboudjema, Mater. Struct. **44**, 1411 (2011).

[29]Y. F. Fu, Y. L. Wong, C. A. Tang, and C. S. Poon, Cem. Concr. Compos. **26**, 99 (2004).

[30]Y. F. Fu, Y. L. Wong, C. A. Tang, and C. S. Poon, Cem. Concr. Compos. **26**, 113 (2004).

[31]J. Bisschop and J. G. M. Van Mier, Heron **47**, 163 (2002).

[32]M. Wyrzykowski and P. Lura, Cem. Concr. Compos. **35**, 49 (2013).

[33]B. Z. Dilnesa *et al.*, Cem. Concr. Res. **41**, 311 (2011).

[34]B. Weber, M. Wyrzykowski, M. Griffa, S. Carl, E. Lehmann, and P. Lura, in Proceedings of 3rd International Workshop on Concrete Spalling due to Fire Exposure, Paris, France, 2012.

[35]M. Bentahar, R. El Guerjouma, S. Idjimarene, and M. Scalerandi, J. Appl. Phys. **113**, 043516 (2013).

[36]X.-T. Chen *et al.*, Cem. Concr. Res. **39**, 195 (2009).

[37]M. Keshavarz, F. L. Pellet, and B. Loret, Pure Appl. Geophys. **167**, 1511 (2010).

[38]P. Antonaci, C. L. E. Bruno, A. S. Gliozzi, and M. Scalerandi, Int. J. Solids Struct. **47**, 1603 (2010).

[39]R. A. Guyer and P. A. Johnson, *Nonlinear Mesoscopic Elasticity* (Wiley VCH, Weinheim, Germany, 2009).